ADVANCED ELECTRONIC MATERIALS
Open Access
www.advelectronicmat.de

Check for updates

Substrate-Free Transfer of Large-Area Ultra-Thin Electronics

*Hugo De Souza Oliveira, Federica Catania, Albert Heinrich Lanthaler, Alejandro Carrasco-Pena, Giuseppe Cantarella, and Niko Münzenrieder**

Innovation in materials and technologies has promoted the fabrication of thin-film electronics on substrates previously considered incompatible because of their chemical or mechanical properties. Indeed, conventional fabrication processes, typically based on photolithography, involve solvents and acids that might harm fragile or exotic substrates. In this context, transfer techniques define a route to overcome the issues related to the nature of the substrate by using supportive carriers in the electronics stack that mitigate or avoid any damages during the fabrication process. Here, a substrate-free approach is presented for the transfer of ultra-thin electronics (<150nm-thick) where no additional layer besides the electronics one remains on the final substrate. Devices are transferred on several surfaces showing good adhesion and an average performance variation of 27%. Furthermore, a sensor bent to a radius of 15.25µm, shows variation in performance of 5%. The technique can also be sequentially repeated for the fabrication of stacked electronics, enabling the development of ultra-thin devices, compliant on unconventional surfaces.

1. Introduction

In recent years, electronics and sensors have been shifting from being bulky and rigid to a thinner and more flexible approach. This shift not only represents a new frontier in the design and development of innovative devices but a new perspective on cost-efficient fabrication techniques.[1] Differently from rigid electronics, thin-film and flexible electronics are able to maintain their functional characteristics even if they are not in their original mechanical state.[2,3] They have made possible new applications[4] on deformable optoelectronics,[5] transient,[6] curvilinear electronics,[7] wearable devices for health diagnostics and artificial intelligence,[8] power source devices,[9] transparent electronics,[10] and sensors.[11,12]

Traditionally, thin-film electronics and sensors are fabricated through a lithography process directly carried out on polymeric substrates, like polyimide (PI), polydimethylsiloxane (PDMS), polymethyl methacrylate (PMMA), and polyethylene terephthalate (PET), as they endow the devices with mechanical flexibility and stable electronics performance.[13] However, for some applications, the desired substrate might not be compatible with the fabrication process, either because it cannot withstand the chemical and the temperature conditions during the realization of the devices, or it cannot meet the handling and the fabrication setup requirements.[4] Therefore, transfer techniques have been developed to transfer the electronics from a donor substrate, which is compatible with all the fabrication steps, to a target substrate, also named receiver.

In general, transfer techniques consists in separating the fabrication process from the receiver substrate through independent steps to bypass their incompatibilities.[4] They allow for the exploration of many unconventional properties of these substrates, such as flexibility,[14] low cost,[1] biocompatibility,[15] and biodegradation.[16] Among the many existing transfer techniques,[15–19] the use of elastomeric tapes or stamps is widely adopted for transferring electronics to planar surfaces.[20,21] It generally consists in weakening the adhesion between the electronics and the donor substrate through selective etching using harsh chemicals,[18] water,[16] or thermal melting,[17] which dissolves a sacrificial layer, and later transferring to a receiver substrate. Similarly, water transfer printing (WTP) is another technique that has been used to transfer electronics to 3D complex large-area surfaces. This process consists in fabricating ultra-thin electronics on top of a dissolvable layer, for example, polyvinyl alcohol (PVA), which is later positioned on the surface of a water bath. The water dissolves the PVA layer, causing the electronics to float. Then, a solid 3D surface is slowly dipped in the water, adhering the electronics onto its surface.[19,22] Additionally, the liquid film transfer printing (LTP) is a technique that enables the fabrication of electronics without any

H. D. S. Oliveira, F. Catania, A. H. Lanthaler, A. Carrasco-Pena, G. Cantarella, N. Münzenrieder
Faculty of Engineering
Free University of Bozen-Bolzano
Bozen-Bolzano 39100, Italy
E-mail: niko.muenzenrieder@unibz.it

G. Cantarella
Department of Physics
Informatics and Mathematics
University of Modena and Reggio Emilia
Modena 41125, Italy

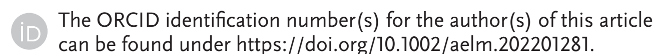
The ORCID identification number(s) for the author(s) of this article can be found under https://doi.org/10.1002/aelm.202201281.

© 2023 The Authors. Advanced Electronic Materials published by Wiley-VCH GmbH. This is an open access article under the terms of the Creative Commons Attribution License, which permits use, distribution and reproduction in any medium, provided the original work is properly cited.

DOI: 10.1002/aelm.202201281

 © 2023 The Authors. Advanced Electronic Materials published by Wiley-VCH GmbH

2199160x, 2023, 9, Downloaded from https://onlinelibrary.wiley.com/doi/10.1002/aelm.202201281 by University Modena, Wiley Online Library on [20/10/2023]. See the Terms and Conditions (https://onlinelibrary.wiley.com/terms-and-conditions) on Wiley Online Library for rules of use; OA articles are governed by the applicable Creative Commons License

damage and can be used with receiver substrates of different materials, patterns, and sizes.[23] Here, the electronics is fabricated on top of a silicon wafer containing a layer of PMMA. Then, an inorganic developer solution is used to hydrolyze the bonds between the PMMA and the silicon wafer, causing the PMMA layer to ascend and float on the liquid surface. Afterward, the PMMA layer is planked up and transferred to the receiver substrate. Although these techniques have been largely used, normally a thin intermediate substrate layer remains between the device and the target surface, which might represent an issue for applications where the contact between the surfaces is necessary.[24,25] To address this adversity, some applications focused on using transferring techniques without an intermediate substrate, resulting in substrate-free devices.

The substrate-free transfer technique presents several advantages compared to conventional substrate-dependent techniques. For example, the absence of an intermediate substrate layer makes possible a better conformability of the electronics to uneven receiver substrates,[19,22] as no substrate layer will influence the deformation of the electronics. It also allows for adequate electrical contact and increased thermal contact conductance between the electronics and the substrate surfaces since no insulating substrate will affect the behavior of the electronics.[25] It enables the realization of multilayered metal-based devices by assembling the layers on top of each other without any substrate to hinder the contact between them.[18,23] Moreover, this technique also represents an environmentally-friendly approach to the fabrication of flexible electronics because some polymer layers can be dissolved and reused, such as PMMA,[26–28] reducing electronic waste during the fabrication steps and the disposal of devices.[29,30] Nevertheless, some limitations should also be considered. For example, wrinkles and deformations might occur in the device during the transfer process because there is no substrate to keep it mechanically stable in the fabrication process. Therefore, larger structures are harder to transfer, as it becomes challenging to position them on the receiver. They can also break or fold onto themselves, affecting the device's integrity and behavior.[19,22] Moreover, the transfer process can be limited by the material that constitutes the receiver substrate. For example, conductive receiver substrates would not benefit from this process if the electronics is composed of conductive layers, which means an insulating substrate would be required. Most applications exploring substrate-free electronics are related to acquiring human body signals, such as epidermal and implantable electronics systems.[31–33] Furthermore, few approaches developed substrate-free electronics on 3D complex large areas,[19,22] as they are hard to achieve and involve processes that depend on visual alignment.[19,22]

Herein, we present a novel technique for substrate-free transfer of several intricate-shaped ultra-thin temperature sensitive devices. The electronics fabrication is performed on a silicon wafer where devices are sandwiched between two soluble layers. This allows for a large-scale transfer of the electronics, enabling the adhesion on top of complex 3D arbitrary surfaces without any intermediate substrate layers, proving the suitability of the process for the utilization of novel and unconventional substrates. Differently from the LTP technique,[23] there is no intermediate layer between the devices and the substrates. The devices remained functional even with the presence of wrinkles. Electrical measurements were performed before and after the transfer, showing an average resistance variation of 27%. After two months of being kept in standard environmental conditions, the average measured resistance showed a variation of -8% from the values originally obtained after transfer. Moreover, the ability to conform to small bending radii of 15.25µm was demonstrated, proving that this method preserves the mechanical stability of the ultra-thin devices while achieving adhesion to complex surfaces. Furthermore, we also presented the capability of the proposed approach in building bi-layered devices where two metal layers were subsequently transferred and aligned on top of each other for the improvement of device functionality.

2. Results and Discussion

Figure 1 displays the schematic of the proposed approach for substrate-free transfer of ultra-thin devices. As shown in Figure 1a, a 3-inch silicon wafer was employed as a temporary carrier for the fabrication of sensors. The wafer was coated with 100 nm thick PVA, a water soluble polymer, acting as a first sacrificial layer in the transfer process.[21] Temperature sensors and thermistors made from 100nm copper (Cu) and 100nm Cu/50nm amorphous indium-gallium-zinc-oxide (a-IGZO), respectively, were fabricated on top of the PVA. Before coating the sensors with the second sacrificial layer, electrical measurements of the devices were performed in a probe station. Afterwards, they were coated with 1.5µm thick PMMA layer. This was chosen because of its solubility in organic solvent, e.g. acetone, while being resistant to water.[31] In turn, this allowed for the complete dissolution of the PVA with no influence on the PMMA. As shown in Figure 1b, the silicon chip with thin-film sensors encapsulated between the two dummy layers was immersed in a water bath to dissolve the PVA. After the sacrificial layer dissolution was completed, thin-film sensors underneath the PMMA layer were completely detached from the silicon wafer as depicted in Figure 1c. At this stage, the floating membrane was ready to be transferred onto any unconventional substrate. As first experiment, a polyimide foil was used to fish the membrane (Figure 1d) which was subsequently rinsed with acetone to dissolve the PMMA leading to substrate-free electronics (Figure 1e). To evaluate the effect of the transfer technique on the performance of the devices, electrical measurements of both temperature sensors and thermistors were conducted when the devices were still on the silicon chip and after the transfer on polyimide. Although all the fabricated devices were measured before and after the transfer, the characterization of only two representative devices, a temperature sensor and a thermistor, are reported.

Figure 2a shows the measured temperature sensor after the fabrication on the silicon wafer, whereas Figure 2b is a picture of the device after being fished with a polyimide foil. The current–voltage sweep characteristic of the temperature sensor is reported in Figure 2c. As expected, the sensor showed a linear behavior with a resistance of 27.3Ω lower than the one measured on the silicon carrier of 39.9Ω. This led to the assumption that the PMMA membrane and the metal underneath undergo compressive strain during the dissolution of the PVA as the elongation of metal will induce an opposite response in the

 © 2023 The Authors. Advanced Electronic Materials published by Wiley-VCH GmbH

2199160x, 2023, 9, Downloaded from https://onlinelibrary.wiley.com/doi/10.1002/aelm.202201281 by University Modena, Wiley Online Library on [20/10/2023]. See the Terms and Conditions (https://onlinelibrary.wiley.com/terms-and-conditions) on Wiley Online Library for rules of use; OA articles are governed by the applicable Creative Commons License

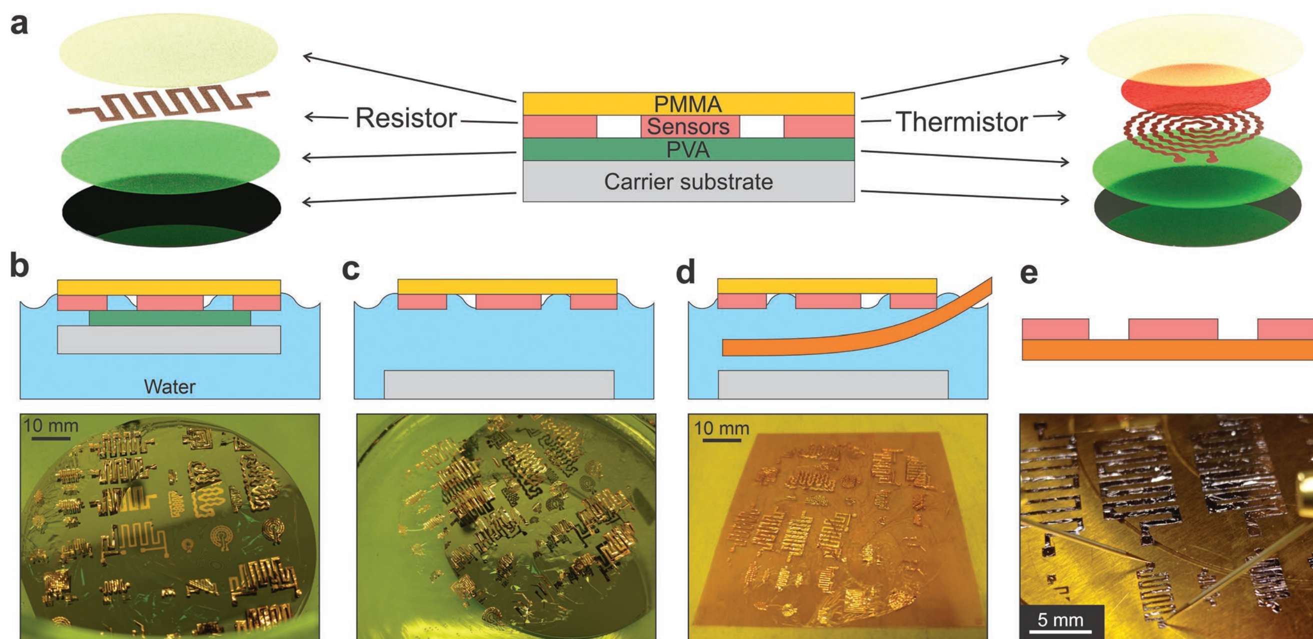

Figure 1. Schematic representation of the proposed zero-substrate transfer technique. a) Representation of the fabricated thin-film devices embedded between the two sacrificial layers (PVA and PMMA) on a carrier substrate (center). Exploded view of temperature sensors (left) and thermistors (right) fabricated by sputtering deposition: temperature sensors are made of 100 nm Cu; the thermistors are made of 100nm Cu/50nm IGZO. b–e) Schematic and photographs of the process flow for temperature sensors fabricated on a 3-inch wafer carrier: (b) PVA dissolution starts from the edges of the sample when immersed in a water bath; (c) the thin-film sensor underneath the PMMA membrane floats on the water surface after being released from the carrier substrate when the PVA is completely dissolved; (d) the membrane is fished with the receiver substrate (a polyimide foil in the presented case); (e) the PMMA is removed by rinsing the foil with acetone (top), so the substrate-free sensors can be characterized afterwards (bottom).

conductivity.[34] This was confirmed by comparing the overall size of the structures before and after transfer leading to a ≈1% shrinkage in the horizontal and vertical directions of the device (see Figure S1, Supporting Information). Accordingly, damages to the structure can be excluded. The thermistor is shown in Figure 2d,e, before and after the transfer, respectively. Also

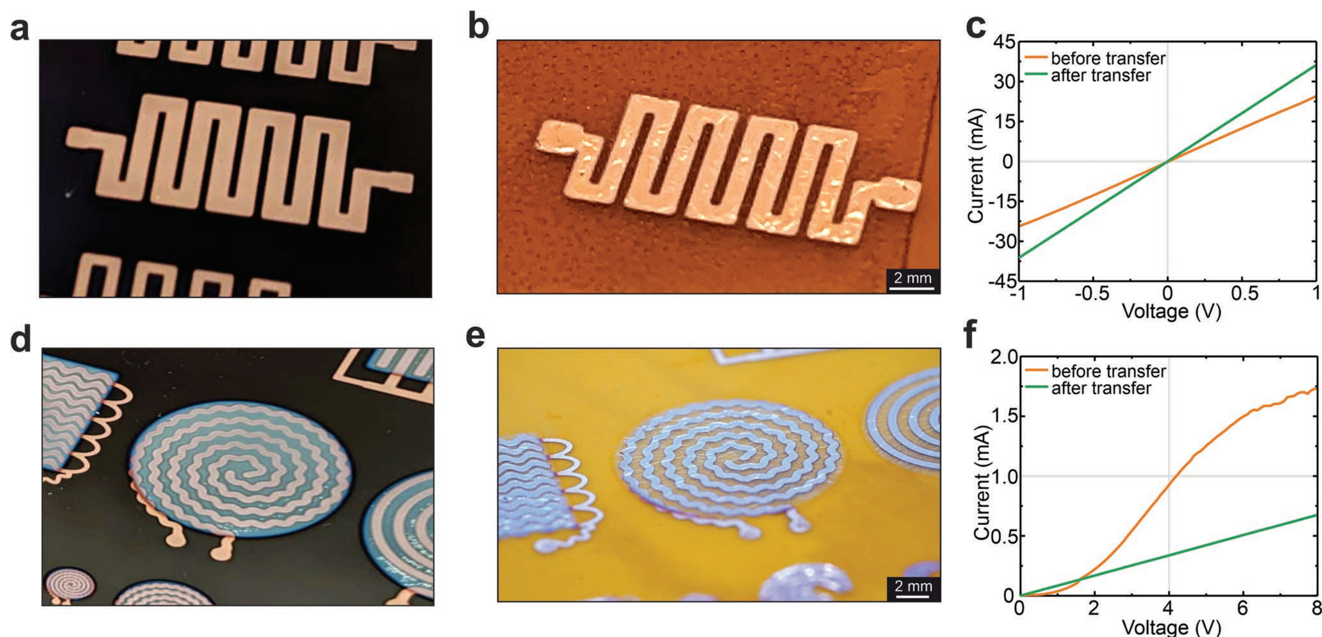

Figure 2. Temperature sensors and thermistors before and after the transfer process. a) Pictures of a representative temperature sensor fabricated on a silicon wafer before spin-coating PMMA and b) after being fished with a polyimide foil. The picture shows the device after PMMA has been removed with acetone. c) Current–voltage sweep curves of the temperature sensor before (Figure a) and after (Figure b) the transfer. d) Pictures of a representative thermistor fabricated on a silicon wafer and e) after being fished with a polyimide foil. The picture shows the device after PMMA has been removed with acetone. f) Current-voltage sweep curves of the thermistor before (Figure d) and after (Figure e) the transfer.

 © 2023 The Authors. Advanced Electronic Materials published by Wiley-VCH GmbH

this device was characterized in both conditions (Figure 2f) in a voltage range (from 0 to 8V). The wider range compared to the sensor one (from -1 to 1V) was chosen to appreciate the non-linear response of the thermistor showing the decrease in resistance as the voltage increases for the measurement before the transfer (orange curve). The average resistance evaluated in the measured range was 10.5kΩ. After the transfer, the current-voltage curve displayed an ohmic-like behavior and the resistance increased to 11.7kΩ (green curve). The performance changes can be addressed to two main parameters influencing the IGZO response. On one side, the PMMA needs a baking step after being spin-coated on top of the devices (see Experimental Section). Since it is reported that annealing processes affect the electrical response of the IGZO increasing its conductivity with temperature,[35] this can explain the ohmic-behavior observed after the transfer, considering the PMMA baking acting as post-annealing for the IGZO layer. On the other side, the dropping down of the current was addressed to the compressive strain on the IGZO layer.[36]

Micrographs of both temperature sensor and thermistor after transferring on polyimide and rinsing with acetone to dissolve the PMMA are reported in **Figure 3**a,b, showing the presence of randomly-oriented wrinkles overall the surface of the devices that induced a shrink in the structures. The appearance of the wrinkles was addressed to the effects of spin-coating and baking processes of the polymers. As reported elsewhere,[37] built-in strain is developed on polymeric layers when spin-coated on a silicon carrier due to thermal expansion. As consequence, the formation of wrinkles observed during the PVA dissolution is associated to the relieved stress in the PMMA layer (see Figure S2, Supporting Information). This, in turns affected the structure of the devices underneath leading to variation in their performance as described for both the sensor and the thermistor. Figure 3c reports the difference in the resistance change for several sensors tested before and after transfer onto the polyimide foil. The common trend observed was a reduction of the resistance values after the transfer with an average difference of 27% from the values before the transfer. Nevertheless, there were outliers showing an opposite trend (see Table S1, Supporting Information). This behavior is attributed not only to the orientation of the wrinkles, but also to the different geometries, both design and size, of the fabricated devices. However, it was possible to evaluate the suitability of the process in preserving the conductivity of the devices. Furthermore, electrical measurements of the same samples stored in ambient conditions for a period of two months after transfer were performed, as reported in the same graph. The values differed from the measurements after the transfer by an average of -8% suggesting the stability of the devices in ambient conditions.

The temperature response of the two devices was also analyzed by measuring the resistance variation from room temperature (RT) ≈20°C up to 85°C. As reported in **Figure 4**a the resistance of the temperature sensor increased with increasing temperature, while decreased when cooling down the device. The temperature coefficient of resistance evaluated as the average between the heating and the cooling ramps was of 0.0023°C^{-1}. The difference with the expected value for Cu of 0.0039°C^{-1} was addressed to the fabrication process as substrate and material thickness can affect the coefficient.[38] The thermal response of the thermistor is reported in Figure 4b, exhibiting a reduction of the resistance with increasing temperature, while becoming less conductive when cooling down. Indeed, the thermistor provided a negative temperature coefficient of resistance of -0.0017°C^{-1} evaluated as the average between the heating and cooling processes. This was also in line with the annealing effect on the after-transfer performance of the thermistor shown in Figure 2f. Furthermore, the device response resulted in better sensitivity to temperature variation since the resistance changed from 25.4Ω down to 7.6Ω when heating, while the temperature sensor resistance variation was of 3.6Ω only from 24.1Ω up to 27.7Ω. On the other hand, the thermistor shows a non-linear response to the temperature variation. A temperature coefficient of resistance of -0.0281°C^{-1} was calculated in a low-temperature range from RT up to 30°C, whereas the value of the temperature coefficient of resistance was measured as -0.0118°C^{-1} in a high-temperature range from 60 to 80°C. These values highlighted the major sensitivity of the thermistor to low-temperature variation, observed also in other metal oxide semiconductors-based thermistors, that makes them a preferable choice for temperature responding devices for wearable and on-skin applications.[39,40]

The suitability of the proposed approach to achieve substrate-free thin-film electronics was proved by performing the transfer on unconventional substrates characterized by different morphology, as shown in **Figure 5**.

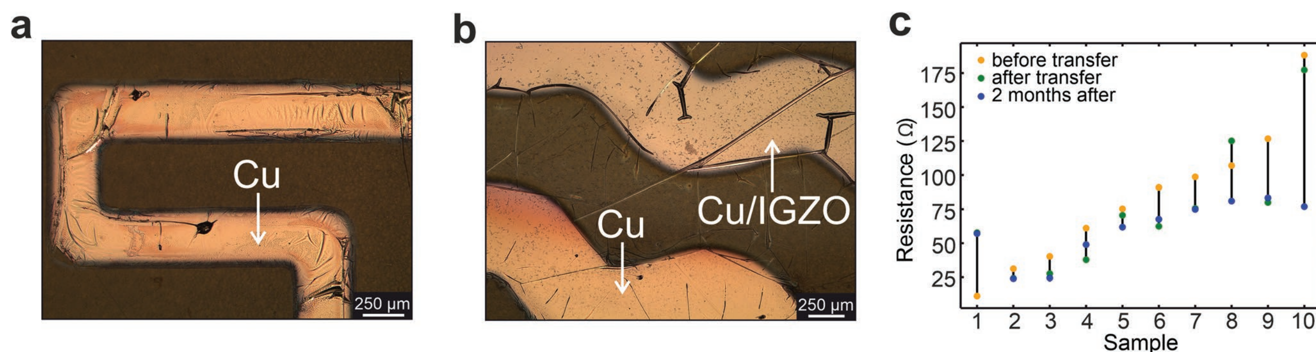

Figure 3. Micrographs of an area of a) a temperature sensor and b) a thermistor after the transfer process showing the presence of wrinkles. c) Resistance values of several temperature sensors characterized by different designs and sizes measured before the transfer, after the transfer, and after two months from the transfer.

 © 2023 The Authors. Advanced Electronic Materials published by Wiley-VCH GmbH

2199160x, 2023, 9, Downloaded from https://onlinelibrary.wiley.com/doi/10.1002/aelm.202201281 by University Modena, Wiley Online Library on [20/10/2023]. See the Terms and Conditions (https://onlinelibrary.wiley.com/terms-and-conditions) on Wiley Online Library for rules of use; OA articles are governed by the applicable Creative Commons License

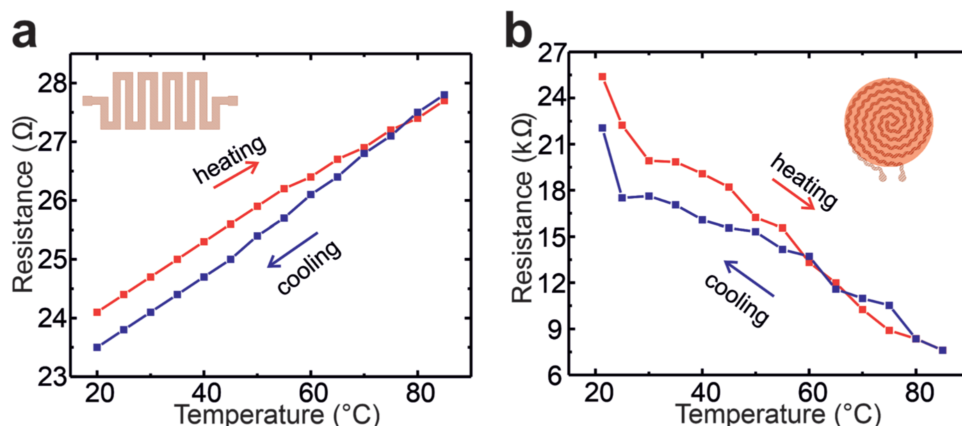

Figure 4. Thermal response of a) temperature sensor and b) thermistor, as shown in the schematic (insets). The devices were characterized after transfer on a polyimide foil.

Since the surface area of the target substrates was smaller than the large area of the fabricated sensors (3-inch), the experiments were performed starting from the manufacturing of the devices on a polyimide foil from where single sensors were cut. Differently from the approach previously presented, each device on the polyimide foil was attached on glass carrier to favor the sinking in water and facilitate the release from it after the PVA dissolution (see Figure S3, Supporting Information). Afterward, the fishing was performed by submerging the receiver's surface. The ultra-thin structures showed good adhesion on all the objects, whereas the irregularity of the volcanic rock led to a peeling-off after the rinsing in acetone (see Figure S4, Supporting Information). To evaluate the mechanical stability of the transferred devices, the resistance of the sensor on the knife was measured as the geometry of the blade was characterized by a radius of curvature of 15.25µm. It was obtained that the resistance changed from 41.2Ω before the transfer to 39.2Ω after the transfer, respectively. This variation of less than 5% in the resistance was attributed to the fact that only a small area of the device was wrapped around the blade, as shown in Figure 5f. By simulating the fishing of the sensor with a knife coming from the bottom in a straight-vertical displacement at the axis of symmetry, it was obtained that the wrapped area in the blade of the knife presented an average strain of only 0.03% deformation mainly at the edges of the channels (Figure 5g). The combination of the small deformed area in the overall structure of the

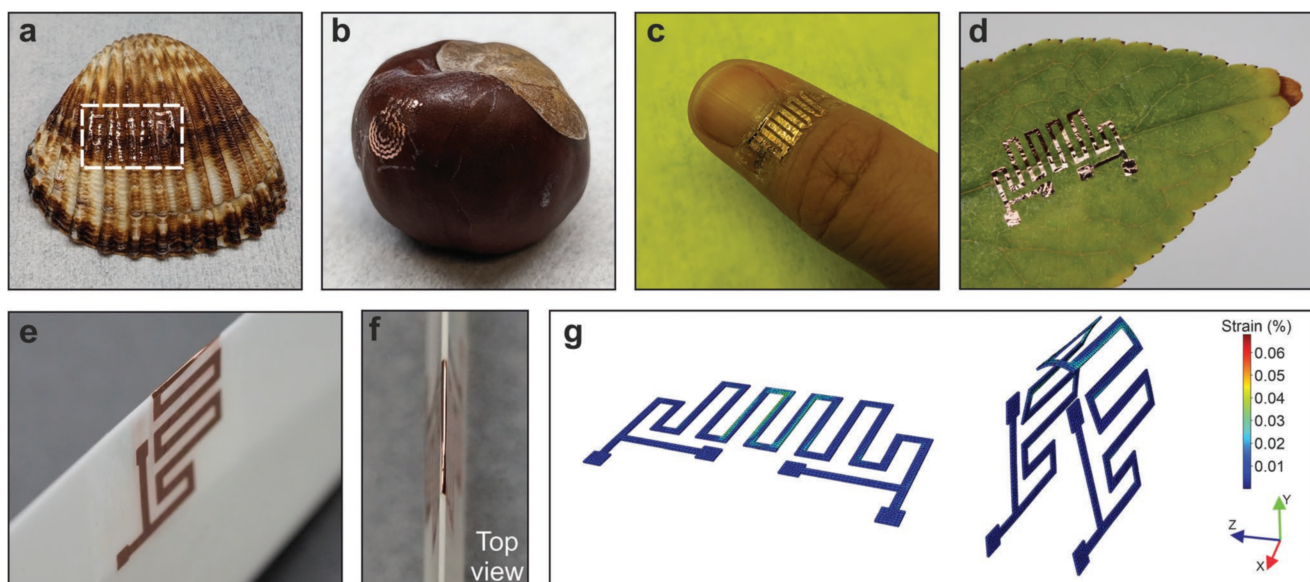

Figure 5. 100nm thick temperature sensors transfer on unconventional substrates. After the PVA dissolution, a) a shell, b) a chestnut, c) a finger, d) a leaf, e) a knife, and f) top view picture showing the temperature sensor wrapped around the blade) were used to fish the sensors. The pictures represent the sensors after PMMA being removed in acetone. The devices showed high conformability to the different morphology of the objects. g) Numerical simulation using finite element analysis of the strain field of the sensor transferred to the blade of a knife. It shows an average strain of 0.03% mainly found in the edges of the channels closer to the contact area with the knife sharp edge. The left-most figure shows the distribution of strain in an undeformed shape to appreciate both sides of the sensor. The right-most part shows the deformed sensor when fished from the bottom using as the contact point the plane of symmetry of the geometry.

© 2023 The Authors. Advanced Electronic Materials published by Wiley-VCH GmbH

2199160x, 2023, 9, Downloaded from https://onlinelibrary.wiley.com/doi/10.1002/aelm.202201281 by University Modena, Wiley Online Library on [20/10/2023]. See the Terms and Conditions (https://onlinelibrary.wiley.com/terms-and-conditions) on Wiley Online Library for rules of use; OA articles are governed by the applicable Creative Commons License

ADVANCED ELECTRONIC MATERIALS
Open Access
www.advelectronicmat.de

2199160x, 2023, 9, Downloaded from https://onlinelibrary.wiley.com/doi/10.1002/aelm.202201281 by University Modena, Wiley Online Library on [20/10/2023]. See the Terms and Conditions (https://onlinelibrary.wiley.com/terms-and-conditions) on Wiley Online Library for rules of use; OA articles are governed by the applicable Creative Commons License

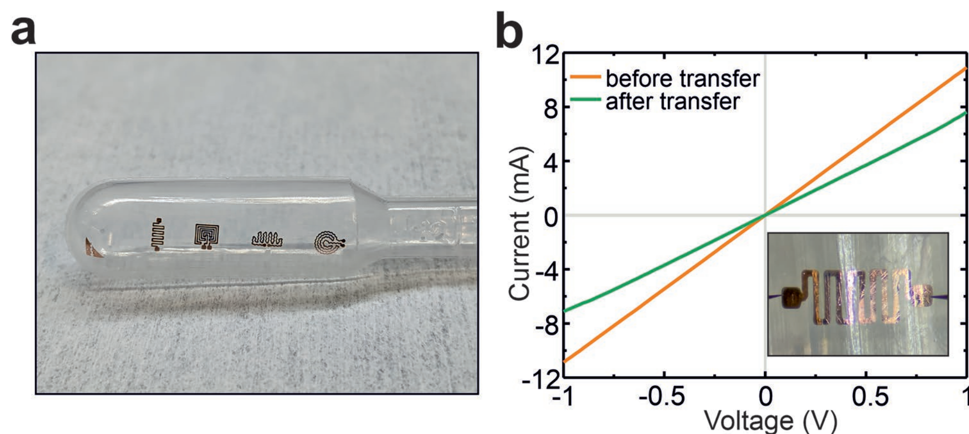

Figure 6. a) Array of four temperature sensors simultaneously transferred on a pipette. b) Electrical measurements of a representative temperature sensor on the pipette (insets) before and after the transfer.

device and the low percentage of strain that was obtained numerically served as an indication that the resistance of the device was not affected by any distortion in the structure since the geometry remained relaxed after the transfer on this particular surface.

An array of four devices was also transferred on a pipette, as shown in **Figure 6**a. These sensors consisted of different geometries with the smallest trace width of 100µm. The current-voltage curves of the left-hand side temperature sensor before and after the transfer on the pipette are reported in Figure 6c, as a representative device. An increase in the resistance was denoted with variations from 90.7 to 134.0Ω, consistent with the sensors performance of Figures 2c and 3c.

To explore the possibility of building multilayer structures, a two-layers temperature sensor was fabricated by 2-transfer process to evaluate the capability of building electronics through a layer-by-layer transfer. To achieve this, a device was transferred on polyimide with the PMMA layer completely removed. Afterwards, this device was used to fish a second sensor with the same dimensions and geometry floating on the water surface, as shown in **Figure 7**a.

Sensor 2 was manually aligned on top of 1. The resistance value of the 2-layer structure was measured as 22.5Ω that, compared with the resistance measured after the first transfer of Sensor 1 of 51.2Ω, results in a 50.4% decrease,

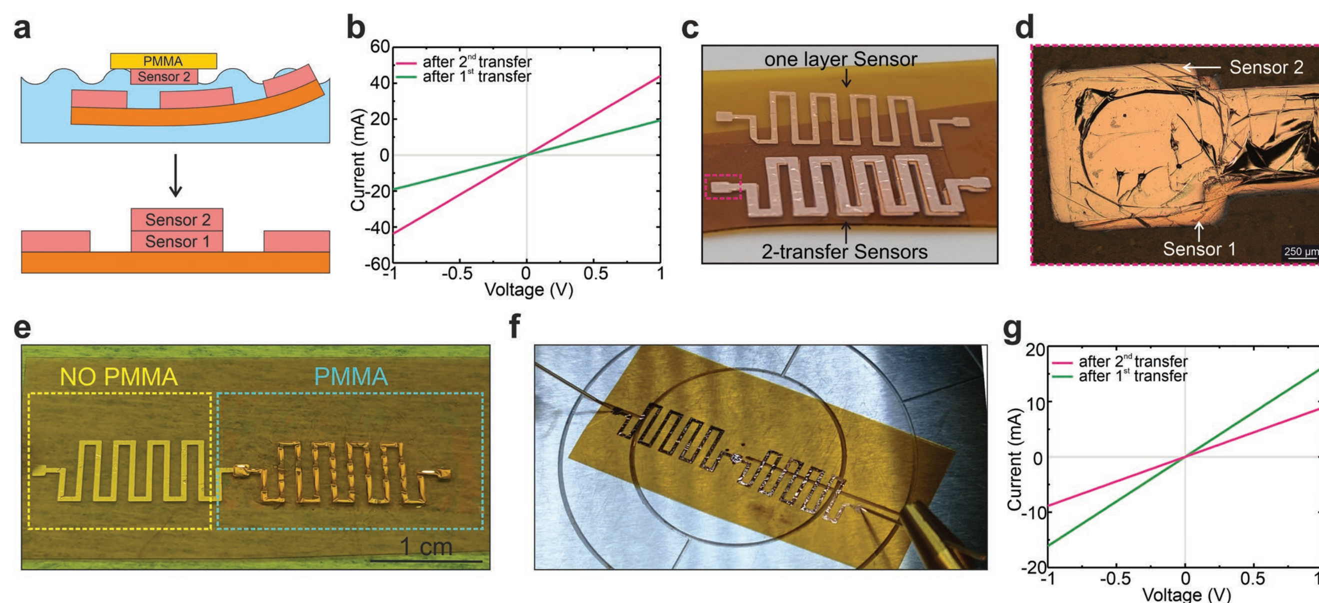

Figure 7. 2-transfer process. a) Schematic of the process: a single temperature sensor is released from the PVA and fished by using a polyimide foil with already transferred devices. b) Electrical measurements of the temperature sensor after the first transfer and the second one. c) Picture of the 2-transfer sensors and d) micrograph of the left-side pads. e) Picture of the series connection of two resistance showing the difference between the first transfer sensor after PMMA removal (left) and the second transferred sensor with PMMA (right). f) The external pads are contacted with the needles to perform the electrical measurements after PMMA was removed overall the device. g) Electrical measurements of the sensors after the first transfer and the second one.

 © 2023 The Authors. Advanced Electronic Materials published by Wiley-VCH GmbH

ADVANCED ELECTRONIC MATERIALS
Open Access
www.advelectronicmat.de

as reported in Figure 7b. This is in line with the expected results since the two devices consisted of 100nm thick Cu each. Thus, the resistance was almost halved because of the double cross-sectional area. In turn, this confirmed the dissolution of the PMMA and the proper adhesion of the two metal layers. A comparison between a single layer and a two-layer sensor is shown in Figure 7c, whereas the micrograph in Figure 7d represents the left-side pads overlapping in the bilayer structure. An average horizontal misalignment of 235µm and a vertical one of 338µm were measured in the whole structure. The observed displacement is due to to the hand alignment of the thin membrane (<2µm thick) performed in water making a precise stacking of the sensor challenging. Even though works showing a highly accurate stacking process based on multi-layer transfer approaches have been presented,[41–43] the fabrication layers always remain as part of the final device. Compared to these techniques, the advantage of the proposed approach offers the possibility of building substrate-free stacked devices with no supporting interlayers. The technique was also tested to build a series connection of two resistances. As before, two sensors with the same design were chosen and transferred one after the other. Figure 7e shows the connection between the two resistance after the second transfer highlighting that PMMA is still covering the second transferred sensor (left device). After rinsing in acetone the whole structure, the electrical measurements were performed as reported in Figure 7f. A resistance of 111.7Ω was obtained from the series connection that is almost double the resistance value of the first transferred device (61Ω), as presented in Figure 7g. The misalignment measured at the overlapping pads was 211µm along the x-axis and 161µm along the y-axis (see Supplementary Video S3, Supporting Information), less than the previous stacked devices since the overlapping was done for the pads only to make the connection.

3. Conclusion

In this work, a transfer technique approach was demonstrated for the fabrication of substrate-free sensors, Cu-based temperature sensors and Cu/IGZO-based thermistors. This process is based on the dissolution of the sacrificial PVA and PMMA layers that hold the structures during their fabrication and transfer stages. Printed devices of different sizes, geometries, and patterns were successfully transferred while preserving their functionality. Additionally, devices were transferred on unconventional substrates showing self-adhesion and adaptability to surfaces, including the blade of a knife having a bending radius of 15.25µm. This technique allows for the fabrication of multi-layer devices by the stacking of structures. The connection in series between two single sensors was also presented suggesting the possibility of building circuits by crossing single devices. Overall, this substrate-free transfer approach offers a route for the fabrication of ultra-thin electronics on novel and unconventional substrates that otherwise could not be used with standard electronics fabrication.

4. Experimental Section

Electronics Fabrication: A 3-inch silicon wafer was employed as a carrier for the preparation of the thin-film sensors. The wafer was cleaned in acetone and isopropanol bath for 5 min, respectively, and then baked on a hot plate. Then, it was coated with a polyvinyl alcohol (PVA, 4.7% concentration) layer spin-coated at 4000 rpm for 60 s and baked at 100°C for 120 s. Afterward, temperature sensors were made of 100 nm Cu deposited by DC sputtering at room temperature, whereas thermistors were made of 100 nm Cu followed by 50 nm IGZO deposited from a ceramic target (1:1:1:4) by RF sputtering at room temperature. The structuring of the electronics was done by shadow mask process during the materials deposition. Although the maximum resolution of the shadow mask is 100µm, the process was chosen instead of other structuring techniques, for example, photolithography, to prevent the possible deterioration of PVA due to wet etching steps because of its water solubility. At this point, the devices were characterized before the transfer. Finally, 1.5µm polymethyl methacrylate (PMMA, 9% concentration in anisole) were spin-coated in two steps: a first step at 500 rpm for 10 s and a second step at 3000 rpm for 60 s. Then, the samples were baked at 100°C for 300 s.

Transfer Technique: The dissolution of the PVA layer of the thin-film sensors fabricated on a silicon carrier was performed by sinking the sample in a water bath. To facilitate the release, the level of water was kept low so the membrane could easily flow on the water surface. Once the PVA was completely dissolved, the sensors underneath the floating PMMA membrane were fished using a 50µm thick polyimide foil. The sample was gently dried using a nitrogen gun and then left under the fume hood. Afterward, it was rinsed with acetone to remove the PMMA and washed with isopropanol. To transfer the electronics on the unconventional substrates, a polyimide foil was used as a carrier for the realization of the sensors. The replacement of the wafer carrier with the polyimide one allows for the cutting of the sample into single sensors. Considering the size and morphology of unconventional substrates being smaller than the polymeric foil (7cm × 7cm), it was preferred to test the technique by fishing single sensors, or few small sensors altogether. As previously described for the 3-inch silicon wafer, the free-standing polyimide foil was coated with PVA. Then, the sensors were fabricated by sputtering deposition and coated with a PMMA layer. The sample was cut after spin-coating the PMMA and attached using double-sided tape on a glass slide to favor the immersion of the lightweight polyimide underwater. Once the PVA was dissolved, the polyimide carrier sank because of the adhesion to the glass slide while the sensors underneath the PMMA membrane floated on the water surface. Then, each final unconventional substrate was immersed in water and slowly lifted up to favor the adhesion of PMMA with the sensors on top of its surface.

Electrical Characterization: The current–voltage measurements of the devices were done under ambient conditions in a probe station using a Keysight B1500A parameter analyzer. The characterization was performed twice for each sensor: when having the electronics on the carrier (both the silicon wafer and the polyimide) before the PMMA spin-coating, and after the transfer process and PMMA dissolution. The sensors transferred on the pipette were also characterized in the probe station, whereas a multimeter was used to measure the resistance of the temperature sensor wrapped around the knife because of the difficulty to ensure good contact between the probe station needles and the pads of the sensor on the blade. The thermal response of the temperature sensor was analyzed in a climate chamber. The device was attached to a glass slide and copper wires were glued on its contact pads by using a conductive silver paste. Then, the wires were taken out from the climate chamber to perform the measurements through a multimeter. The resistance values were taken once the temperature was stable. The temperature variation effect on the thermistor was analyzed on a hot plate. This was done because the climate chamber acts on the temperature control by also changing the humidity. To prevent the influence of humidity on the IGZO stability, the hot plate was used in a controlled humidity environment (40% RH). In both

© 2023 The Authors. Advanced Electronic Materials published by Wiley-VCH GmbH
2199160x, 2023, 9, Downloaded from https://onlinelibrary.wiley.com/doi/10.1002/aelm.202201281 by University Modena, Wiley Online Library on [20/10/2023]. See the Terms and Conditions (https://onlinelibrary.wiley.com/terms-and-conditions) on Wiley Online Library for rules of use; OA articles are governed by the applicable Creative Commons License

cases, the characterization was done in a temperature range between room temperature up to 85°C with a sweep of 5°C.

Finite Element Analysis: A numerical analysis using the finite element method was performed to simulate the strain distribution on the surface of the structure wrapped around the small radii of the blade of the knife (15.25µm). Abaqus/CAE V6.11 (Dassault Systemes, France) was used to conduct the finite element analysis. A displacement-controlled simulation was setup, using 8-node linear brick, reduced integration (C3D8R) elements for the mesh on a 3D deformable geometry. A displacement along the y-direction to simulate the motion of the knife fishing the floating device. The properties of the material used were the typical elastic mechanical properties for Cu, with Young's modulus of 117GPa, Poisson's ratio of 0.34, and density of 9.40g cm^{-3}.

Supporting Information

Supporting Information is available from the Wiley Online Library or from the author.

Acknowledgements

H.S.O., F.C., A.H.L., and A.C.P., contributed equally to this work and wish it to be known that, in their opinion, the first two authors should be regarded as Joint First Authors. G.C., and N.M. supervised the work. This work was partially funded by the Autonomous Province of Bozen-Bolzano-South Tyrol's European Regional Development Fund (ERDF) Program: project code EFRE/FESR 1140-PhyLab, and the Autonomous Province of Bozen-Bolzano/South Tyrol through the International Joint Cooperation South Tyrol-Switzerland SNF (FLEXIBOTS, grant no.: 2/34).

Conflict of Interest

The authors declare no conflict of interest.

Data Availability Statement

The data that support the findings of this study are available from the corresponding author upon reasonable request.

Keywords

flexible electronics, substrate-free, transfer techniques, ultra-thin electronics

Received: December 2, 2022
Revised: February 9, 2023
Published online: April 17, 2023

[1] M.-G. Kim, M. G. Kanatzidis, A. Facchetti, T. J. Marks, *Nat. Mater.* **2011**, *10*, 382.
[2] H. Yang, W. R. Leow, X. Chen, *Small Methods* **2018**, *2*, 1700259.
[3] H. de Souza Oliveira, A. Nijkoops, M. Ciocca, A. Carrasco-Peña, L. Petti, G. Cantarella, N. Münzerieder, presented at *IEEE Sensors*, IEEE, Dallas, November **2022**.
[4] C. Linghu, S. Zhang, C. Wang, J. Song, *npj Flexible Electron.* **2018**, *2*, 26.
[5] D.-H. Lien, H.-P. Wang, S.-B. Chen, Y.-C. Chi, C.-L. Wu, G.-R. Lin, Y.-C. Liao, J.-H. He, *npj Flexible Electron.* **2018**, *2*, 1.
[6] S.-W. Hwang, H. Tao, D.-H. Kim, H. Cheng, J.-K. Song, E. Rill, M. A. Brenckle, B. Panilaitis, S. M. Won, Y.-S. Kim, Y. M. Song, K. J. Yu, A. Ameen, R. Li, Y. Su, M. Yang, D. L. Kaplan, M. R. Zakin, M. J. Slepian, Y. Huang, F. G. Omenetto, J. A. Rogers, *Science* **2012**, *337*, 1640.
[7] D.-H. Kim, J. Xiao, J. Song, Y. Huang, J. A. Rogers, *Adv. Mater.* **2010**, *22*, 2108.
[8] X.-H. Zhao, S.-N. Ma, H. Long, H. Yuan, C. Y. Tang, P. K. Cheng, Y. H. Tsang, *ACS Appl. Mater. Interfaces* **2018**, *10*, 3986.
[9] J. Peng, I. Witting, N. Geisendorfer, M. Wang, M. Chang, A. Jakus, C. Kenel, X. Yan, R. Shah, G. J. Snyder, M. Grayson, *Nat. Commun.* **2019**, *10*, 1.
[10] F. Catania, M. Ahmad, D. Corsino, N. S. Khaanghah, L. Petti, N. Münzenrieder, G. Cantarella, *IEEE Trans. Electron Devices* **2022**, *69*, 4930.
[11] Z. Liu, B. Tian, B. Zhang, J. Liu, Z. Zhang, S. Wang, Y. Luo, L. Zhao, P. Shi, Q. Lin, Z. Jiang, *Microsyst. Nanoeng.* **2021**, *7*, 1.
[12] H. de Souza Oliveira, F. Catania, G. Cantarella, V. Benedetti, M. Baratieri, N. Münzenrieder, presented at *IEEE Int. Flexible Electronics Technology Conf. (IFETC)*, IEEE **2021**.
[13] F. Catania, H. de Souza Oliveira, P. Lugoda, G. Cantarella, N. Münzenrieder, *J. Phys. D: Appl. Phys.* **2022**, *55*, 323002.
[14] P. Giannakou, M. O. Tas, B. Le Borgne, M. Shkunov, *ACS Appl. Mater. Interfaces* **2020**, *12*, 57207.
[15] J. Park, Y. Lee, H. Lee, H. Ko, *ACS Nano* **2020**, *14*, 12.
[16] C. H. Lee, D. R. Kim, X. Zheng, *Nano Letters* **2011**, *11*, 3435.
[17] C. H. Lee, J.-H. Kim, C. Zou, I. S. Cho, J. M. Weisse, W. Nemeth, Q. Wang, A. C. T. v. Duin, T.-S. Kim, X. Zheng, *Sci. Rep.* **2013**, *3*, 2917.
[18] J. Zhang, Y. Wu, Z. Li, Y. Zhang, Y. Peng, D. Chen, W. Zhu, S. Xu, C. Zhang, Y. Hao, *Sci. Rep.* **2019**, *9*, 15769.
[19] B. Le Borgne, S. Liu, X. Morvan, S. Crand, R. A. Sporea, N. Lu, M. Harnois, *Adv. Mater. Technol.* **2019**, *4*, 1800600.
[20] H. Ko, K. Takei, R. Kapadia, S. Chuang, H. Fang, P. W. Leu, K. Ganapathi, E. Plis, H. S. Kim, S.-Y. Chen, M. Madsen, A. C. Ford, Y.-L. Chueh, S. Krishna, S. Salahuddin, A. Javey, *Nature* **2010**, *468*, 286.
[21] S. H. Jin, S.-K. Kang, I.-T. Cho, S. Y. Han, H. U. Chung, D. J. Lee, J. Shin, G. W. Baek, T.-i. Kim, J.-H. Lee, J. A. Rogers, *ACS Appl. Mater. Interfaces* **2015**, *7*, 8268.
[22] B. Le Borgne, E. Jacques, M. Harnois, *Micromachines* **2018**, *9*, 474.
[23] Y. Chen, X. Liu, Y. Ma, Y. Chen, B. Lu, X. Feng, *Adv. Mater. Interfaces* **2021**, *8*, 2100287.
[24] S. Choi, S. I. Han, D. Jung, H. J. Hwang, C. Lim, S. Bae, O. K. Park, C. M. Tschabrunn, M. Lee, S. Y. Bae, J. W. Yu, J. H. Ryu, S.-W. Lee, K. Park, P. M. Kang, W. B. Lee, R. Nezafat, T. Hyeon, D.-H. Kim, *Nat. Nanotechnol.* **2018**, *13*, 1048.
[25] S. Nie, C. Zhang, J. Song, *Sci. Rep.* **2018**, *8*, 1.
[26] E. Esmizadeh, S. Khalili, A. Vahidifar, G. Naderi, C. Dubois, in *Handbook of Ecomaterials*, Springer, Cham, Switzerland **2018**, pp. 1–33.
[27] X. D. Zhou, S. C. Zhang, W. Huebner, P. D. Ownby, H. Gu, *J. Mater. Sci.* **2001**, *36*, 3759.
[28] C. D. Papaspyrides, S. Gouli, J. G. Poulakis, *Adv. Polym. Tech.* **1994**, *13*, 213.
[29] A. K. Awasthi, J. Li, L. Koh, O. A. Ogunseitan, *Nat. Electron.* **2019**, *2*, 86.
[30] A. Carrasco-Pena, F. Catania, G. Cantarella, M. Haller, M. Nippa, N. Münzenrieder, presented at *IEEE Sensors*, IEEE, Dallas, November **2022**.
[31] Z. Wang, Q. Lu, Y. Xia, S. Feng, Y. Shi, S. Wang, X. Yang, Y. Zhao, F. Sun, T. Li, T. Zhang, *Microsyst. Nanoeng.* **2021**, *7*, 1.
[32] W. Yeo, Y. Kim, J. Lee, A. Ameen, L. Shi, M. Li, S. Wang, R. Ma, S. H. Jin, Z. Kang, Y. Huang, J. A. Rogers, *Adv. Mater.* **2013**, *25*, 2773.

© 2023 The Authors. Advanced Electronic Materials published by Wiley-VCH GmbH

2199160x, 2023, 9, Downloaded from https://onlinelibrary.wiley.com/doi/10.1002/aelm.202201281 by University Modena, Wiley Online Library on [20/10/2023]. See the Terms and Conditions (https://onlinelibrary.wiley.com/terms-and-conditions) on Wiley Online Library for rules of use; OA articles are governed by the applicable Creative Commons License

[33] W. Lee, D. Kim, N. Matsuhisa, M. Nagase, M. Sekino, G. G. Malliaras, T. Yokota, T. Someya, *Proc. Natl. Acad. Sci. U.S.A.* **2017**, *114*, 10554.
[34] J. Jones, S. P. Lacour, S. Wagner, Z. Suo, *J. Vac. Sci. Technol., A* **2004**, *22*, 1723.
[35] M. Estrada, M. Rivas, I. Garduño, F. Avila-Herrera, A. Cerdeira, M. Pavanello, I. Mejia, M. A. Quevedo-Lopez, *Microelectron. Reliab.* **2016**, *56*, 29.
[36] N. Munzenrieder, K. H. Cherenack, G. Troster, *IEEE Trans. Electron Devices* **2011**, *58*, 2041.
[37] G. Cantarella, C. Vogt, R. Hopf, N. Münzenrieder, P. Andrianakis, L. Petti, A. Daus, S. Knobelspies, L. Büthe, G. Tröster, G. A. Salvatore, *ACS Appl. Mater. Interfaces* **2017**, *9*, 28750.
[38] A. I. Oliva, J. M. Lugo, R. A. Gurubel-Gonzalez, R. J. Centeno, J. E. Corona, F. Avilés, *Thin Solid Films* **2017**, *623*, 84.
[39] K. Sim, Z. Rao, Z. Zou, F. Ershad, J. Lei, A. Thukral, J. Chen, Q.-A. Huang, J. Xiao, C. Yu, *Sci. Adv.* **2019**, *5*, eaav9653.
[40] I.-J. Park, C.-Y. Jeong, I.-T. Cho, J.-H. Lee, E.-S. Cho, S. J. Kwon, B. Kim, W.-S. Cheong, S.-H. Song, H.-I. Kwon, *Semicond. Sci. Technol*. **2012**, *27*, 105019.
[41] Y. Mao, Y. Wu, P. Zhang, Y. Yu, Z. He, Q. Wang, *J. Mater. Sci. Technol*. **2021**, *61*, 132.
[42] R. Guo, J. Tang, S. Dong, J. Lin, H. Wang, J. Liu, W. Rao, *Adv. Mater. Technol*. **2018**, *3*, 1800265.
[43] H. Li, Z. Wang, Y. Cao, Y. Chen, X. Feng, *ACS Appl. Mater. Interfaces* **2021**, *13*, 1612.

© 2023 The Authors. Advanced Electronic Materials published by Wiley-VCH GmbH

2199160x, 2023, 9, Downloaded from https://onlinelibrary.wiley.com/doi/10.1002/aelm.202201281 by University Modena, Wiley Online Library on [20/10/2023]. See the Terms and Conditions (https://onlinelibrary.wiley.com/terms-and-conditions) on Wiley Online Library for rules of use; OA articles are governed by the applicable Creative Commons License